Flow Rate Measurement in Flows with Asymmetric Velocity Profiles by Means of Distributed Thermal Anemometry

Arlit, M.; Schroth, C.; Schleicher, E.; Hampel, U.;

Originally published:

May 2019

Flow Measurement and Instrumentation 68(2019), 101570

DOI: https://doi.org/10.1016/j.flowmeasinst.2019.05.004

Perma-Link to Publication Repository of HZDR:

https://www.hzdr.de/publications/Publ-28902

FLOW RATE MEASUREMENT IN FLOWS WITH ASYMMETRIC VELOCITY PROFILES BY MEANS OF DISTRIBUTED THERMAL ANEMOMETRY

Martin Arlit[1], Christoph Schroth[2], Eckhard Schleicher[2] and Uwe Hampel[1,2]
[1] AREVA Endowed Chair for Imaging Techniques in Energy and Process Engineering, Technische Universität Dresden, 01062 Dresden, GERMANY
[2] Helmholtz-Zentrum Dresden-Rossendorf, Institute of Fluid Dynamics, Bautzner Landstraße 400, 01328 Dresden, GERMANY
(Email: Martin.Arlit@tu-dresden.de; Christoph_Schroth@tu-dresden.de; E.Schleicher@hzdr.de; Uwe.Hampel@tu-dresden.de)

ABSTRACT

Flow rate in closed conduits is one of the most frequently measured parameters in industrial processes and in gas and water supply. For an accurate measurement, flow meters typically require a fully developed symmetric flow profile with preferably no radial or tangential velocity components. This is commonly secured by mounting flow meters in a pipe at a sufficiently long distance downstream any change in cross-section or pipe direction. In this paper, we introduce a new approach for flow rate measurement of gases or liquids that employs a novel spatially resolving fluid velocity sensor basing on thermal anemometry. The new principle allows accurate flow rate measurements for non-axisymmetric velocity profiles, even directly after pipe bends, T-junctions or other alterations in the pipe geometry. This is exemplified for air flow in three different pipe bend configurations.

KEYWORDS

Flow rate measurement; installation effects; thermal anemometry grid sensor

NOMENCLATURE

symbol	unit	description	symbol	unit	description
A	m²	area	$\dot{V}$	m³/s	volumetric flow rate
A_ϑ, B_ϑ	K^{-1}, K^{-2}	temperature coefficient of resistance	v	m/s	velocity
a_i, b_i, c_i	A^{-1},$A^{-1}K^{-1}$, $A^{-1}K^{-2}$	temperature calibration parameters			
$C_{1,i}$, $C_{2,i}$, n	1	velocity calibration parameters	*greek*		
D	m	pipe diameter	α	W/(m²·K)	heat transfer coefficient
f	1	relative deviation	$\Delta\vartheta$	K	overheating
g	1	weighting factor	ϑ	°C	temperature
I	A	electrical current			
L	m	length	*subscripts*		
P_{el}	W	Joule heating power	h		heating
p	Pa	pressure	*i*		index of RTD
$\dot{Q}_{\mathrm{c}}$	W	convective heat flux	f		fluid
$\dot{Q}_{\mathrm{t}}$	W	thermal conduction heat flux	0		reference
R	Ω	electrical resistance	min		minimum
r	m	radius	max		maximum
U	V	voltage	nom		nominal

1 INTRODUCTION

Flow rate is one of the most often measured parameters in industry and public utility infrastructure. Applications are in the production and distribution of natural and technical gases, the monitoring and controlling of chemical plants and processes, air supply in firing plants or in room air conditioning. Especially when there is a billing relevance, requirements on accuracy are very high. Flow rate can be measured in various ways. Examples are orifice, nozzle or Venturi meters, ultrasonic meters, vortex meters, magnetic-inductive meters, Coriolis flow meters, mechanical-volumetric meters and thermal anemometry meters. Beside uncertainties coming from the instrument itself, the actual flow conditions in the metering device are of great importance. Almost all commercial flow meters measure volumetric or mass flow in an integral way and thereby rely on some symmetry of the flow in the pipe section. Pipe geometry changes, such as in bends, T-junctions or armatures, may lead to swirling or asymmetric flow conditions. Hence, the mounting position is of highest significance. To illustrate the problem Figure 1 shows the flow field downstream of an elbow in a pipe with an inner diameter of $d = 0.08\ \mathrm{m}$. This flow was simulated with the CFD code ANSYS Fluent with an SST $k-\omega$ turbulence model for an averaged air velocity of $\bar{v} = 4\ \mathrm{m/s}$. Here, one can clearly see the asymmetric velocity field behind the bend in the cross-section.

A sufficiently developed and symmetric flow is typically secured by having a straight pipe with a certain length-to-diameter ratio L/D upstream of the meter. For example, an orifice flow meter with an orifice plate of area ratio $\beta = 0.6$ (ISO 5167) requires an L/D ratio of 42 in case of a 90° bend. This length can be reduced to $L/D = 30$ when a flow straightener is used [1]. Martin investigated the deviation for shorter straight inlet lengths and found a shift in the discharge coefficient of up to -5.8 % for $L/D = 2$ ($\beta = 0.64$) [2]. Another approach is the formation of defined flow conditions that are not necessarily symmetric or swirl-free. E. g. Beck and Mazille presented a flow meter with a swirl element upstream of an orifice to create a defined swirl independent of upstream installations [3]. Some flow meters get along with smaller L/D ratios as their measuring principle is more tolerant

to non-ideal flow profiles. For commercial ultrasonic flow meters producers specify $L/D = 10$ for a meter with four measurement paths. Further increase of transmitter-receiver paths numbers can reduce the uncertainty or the required L/D. Ruppel investigated the influence of installation effects for an ultrasonic single path arrangement with variable angular positions [4]. He found a maximum deviation of up to 3.8 % downstream a 90 ° bend at a distance of $L/D = 2$. Holm et al. proposed an approach for shorter L/D ratios that includes a CFD calculation of the flow profile and derivation of proper correction factors [5].
The flow rate may also be derived from a representative local velocity measurement using a local probe, e.g. a Pitot tube, if the flow profile is known. This is again the case for laminar and turbulent flows in a sufficiently long straight pipe. If the profile is not known, the local flow velocity may be measured at several positions in the flow cross-section, e.g. by traversing a single Pitot tube [6]. Alternatively, an averaging Pitot tube can be used [7].

The approach presented in this paper bases on a multipoint measurement of local flow velocity in the flow cross-section and a subsequent area averaging. It is hence somewhat comparable with the single probe traversing technique. However, our approach avoids sequential scanning in the cross-section by introducing a grid of small and minimal intrusive thermal anemometry sensors. In the following, we introduce the sensor principle and show exemplary results for a gas flow in a pipe $L/D = 1$ downstream an elbow, a double elbow and a T-junction.

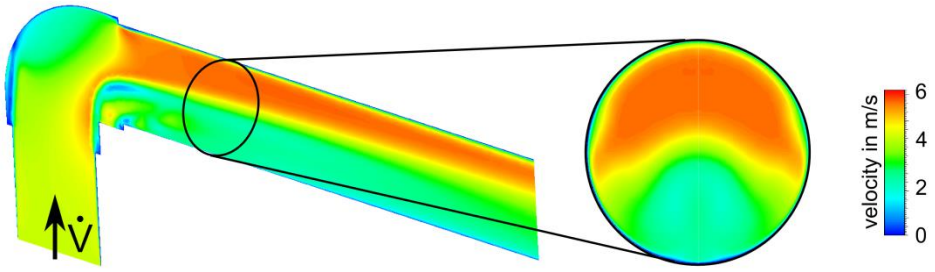

Figure 1. Simulated gas flow field after an elbow in a straight pipe.

2 THERMAL ANEMOMETRY GRID SENSOR

2.1 Principle and Design

The proposed sensor measures fluid velocities via the thermal anemometry principle. For that, we employ resistance thermometer detectors (RTD). For such there is a general polynomial relationship between resistance R and sensor temperature ϑ given as

$$R = \frac{U}{I} = R_0 \cdot [1 + A_\vartheta(\vartheta - \vartheta_0) + B_\vartheta(\vartheta - \vartheta_0)^2 + higher\ order\ terms]. \tag{1}$$

R_0 is the nominal resistance at reference temperature ϑ_0. A_ϑ and B_ϑ are the temperature coefficients of resistance [8]. In thermal equilibrium, the temperature of the sensor is equal to the temperature ϑ_f of the surrounding fluid. Hence, this temperature is measured by applying a small voltage U_f that is just low enough to avoid self-heating and measuring the resulting electrical current I_u through the resistor. Applying a higher voltage U_h leads to significant Joule heating of the resistor with an electrical power $P_\mathrm{el} = U_\mathrm{h}^2/R$. The heat is dissipated into the solid connectors via heat conduction with heat flux $\dot{Q}_\mathrm{t}$ and via heat convection with heat flux $\dot{Q}_\mathrm{c}$. In total this gives the heat balance

$$P_\mathrm{el} = \frac{U_\mathrm{h}^2}{R} = \dot{Q}_\mathrm{t} + \dot{Q}_\mathrm{c}. \tag{2}$$

The convective heat flux is further given by

$$\dot{Q}_\mathrm{c} = \alpha(v)A[\vartheta_\mathrm{h} - \vartheta_\mathrm{f}] \tag{3}$$

with the sensor surface area A and the temperature difference $\Delta\vartheta = \vartheta_\mathrm{h} - \vartheta_\mathrm{f}$ between the heated sensor (ϑ_h) and the bulk fluid (ϑ_f) [9]. The heat transfer coefficient α is a function of the fluid velocity v. To determine the latter, both temperatures ϑ_h and ϑ_f must be known.

For a spatially resolved fluid velocity measurement in a flow cross-section, we arrange a multitude of RTDs in the crossings of a wire grid (Figure 2). This arrangement is referred to as thermal anemometry grid sensor TAGS [10]. To interrogate the RDTs we apply a special matrix excitation-acquisition scheme, which is briefly illustrated below.

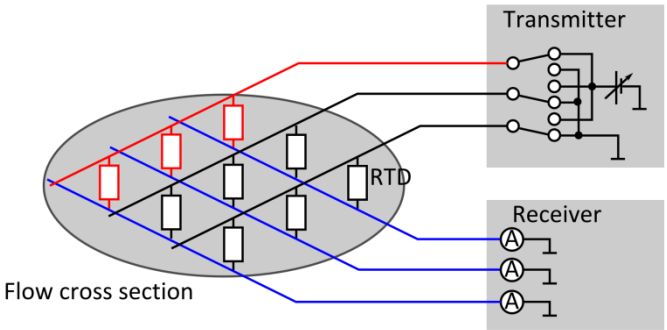

Figure 2. Basic electronic sensor design and illustration of the excitation-acquisition scheme.

The grid arrangement requires constant voltage anemometry as operation mode. For that, a constant voltage U_h is applied to all rows of RTDs. This leads to a heating of the resistors to temperature ϑ_h. Switching U_h to only one row and measuring the electrical current through the resistors gives ϑ_h from eq. (1). This procedure is repeated for all transmitter rows. Subsequent to the heating phase a lower voltage U_f is applied row by row. The resistor returns to the fluid temperature and a second current measurement gives ϑ_f. Having obtained the local fluid velocities at multiple points within the grid the flow rate is calculated via the area-averaging method [11].

For a proof of principle we built a sensor with 16 RTDs. Its design is shown in Figure 3. The wire grid is not equidistant but made in a way to give an equiangular polar arrangement of the RTDs in the cross-section, which is a more representative spatial sampling scheme for a circular cross-section. An important additional element beside the TAGS is a honeycomb flow straightener directly upstream the TAGS [12]. The essential role of this component is to enforce a channel-wise fully-developed laminar flow, which effectively suppresses any geometry-induced as well as turbulent cross-flow and hence improves the overall accuracy. The honeycomb channels have an inner diameter of $2.5\ \mathrm{mm}$ and a length of $30\ \mathrm{mm}$. The areal coverage ratio of the sensor in a subchannel of the honeycomb is 14.7 %.

The RTDs are platinum resistors with a nominal resistance of $100\ \Omega$ at $\vartheta_0 = 0\ °\mathrm{C}$ and dimensions 1.6 mm × 1.2 mm × 0.6 mm, which were soldered into the wire grid. The applied excitation voltages are $U_\mathrm{h} = 2.70\ \mathrm{V}$ and $U_\mathrm{f} = 0.11\ \mathrm{V}$. The signal processing electronics samples are RTD values within 0.5 s. As the thermal relaxation time at $v = 1\ \mathrm{m/s}$ average air flow is about $t_{0.95} = 4\ s$ we intermittently measure ϑ_f and ϑ_h with 15 s distance to secure thermal equilibrium.

The RTDs are equally distributed on two circles with radius r_1 and r_2 (**Fehler! Verweisquelle konnte nicht gefunden werden.**a) with the numbering $i = 1 \dots 8$ and $i = 9 \dots 16$ respectively. For this arrangement we get the two differently shaped area sectors A_1 and A_2 around each RTD, which are shown in Fig. 3. Assuming that the local velocity v_i at sensor i is representative for the whole sector, we can calculate the cross-sectional averaged velocity as

$$\bar{v} = \frac{1}{16}\left(\sum_{i=1}^{8} g \cdot v_i + \sum_{i=9}^{16} (1-g) \cdot v_i\right) \tag{4}$$

with the weighting factor

$$g = \frac{A_1}{A_1 + A_2} = \left(\frac{r_\mathrm{p}}{r_0}\right)^2. \tag{5}$$

There is some freedom in the choice of the radii r_1, r_2 and r_p. We took the advantage of having CFD-flow data available to fix these parameters. Hence, we assessed the simulated flow field downstream the pipe bend for $v_\mathrm{nom} = 4\ \mathrm{m/s}$ and numerically varied both radii in the ranges $10\ mm \leq r_1 \leq 20\ mm$ and $21\ mm \leq r_2 \leq 37\ mm$ in steps of 1 mm until the lowest deviation

between the given averaged velocity $\bar{v}$ and the one calculated with eqs. (4) and (5) had been found. This analysis gave $r_1 = 17\ \mathrm{mm}, r_\mathrm{p} = 23\ \mathrm{mm}, r_2 = 29\ \mathrm{mm}$.

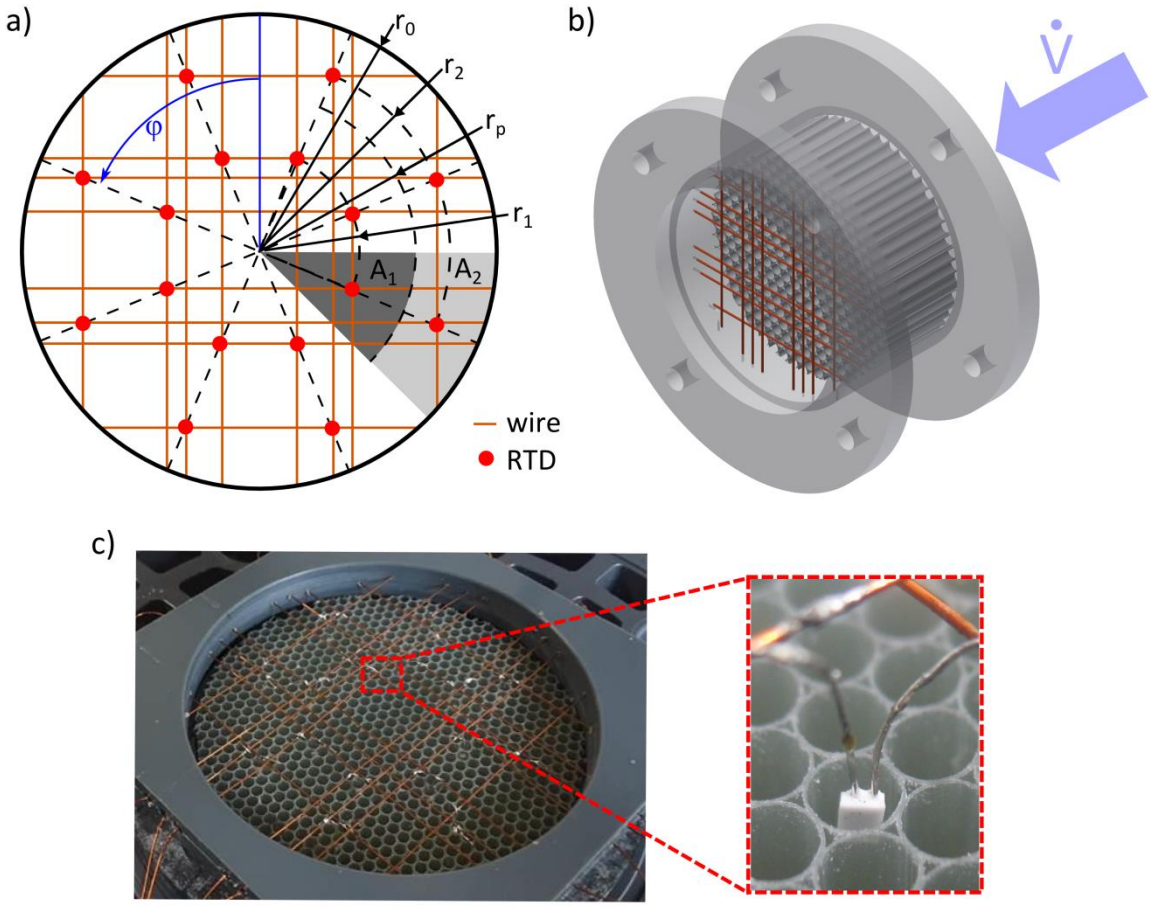

Figure 3. a) Sketch of the RTD arrangement, b) CAD model of the sensor and c) a photo of the sensor with a detail view of one platinum resistor.

2.2 Calibration

Due to the tolerances in active and passive electronic components and uncertainties from wire resistances, a calibration of the sensor is required. This was done in a climate chamber. The temperature ϑ in the chamber was varied in a range between 20 °C and 80 °C in steps of 5 K. The reference temperature in thermal equilibrium was measured with a platinum resistor (class F 0.1) and a precision multimeter KEITHLEY 2700. For each RTD (index i) we determined the coefficients of a second-order polynomial

$$\frac{U_h}{I_i} = a_i + b_i\vartheta + c_i\vartheta^2, \tag{6}$$

which is a different representation of eq. 1. As the relationship between fluid velocity and overheat (eq. 2) is complex and geometry-dependent we also performed a velocity calibration using a fully developed turbulent flow in a straight pipe with a diameter of 0.08 m. Turbulent pipe flow is well suited as is has a flat cross-sectional velocity profile. Directly upstream of the TAGS an open-cell

foam was mounted to reduce low frequency fluctuations of the local velocity. The uniformity of the flow profile was checked with a traversing single thermal anemometry probe. A coefficient of variation $c_v = s/v_{\mathrm{nom}}$ with a standard deviation $s = 0.04\%$ was found. The nominal velocity $v_{\mathrm{nom}} = \dot{V}/A$ was calculated from the flow rate $\dot{V}$ controlled via a mass flow controller and the cross-sectional area of the pipe. It was varied between 0.5 m/s and 4.0 m/s in steps of 0.25 m/s. The relation between the flow velocity and the overheating was fitted by the power function

$$v_i = C_{1,i} + C_{2,i}(\Delta\vartheta'_i)^n \tag{7}$$

with the fitting parameters $C_{1,i}$, $C_{2,i}$ and n.

3 EXPERIMENTS

3.1 Setup

The TAGS-based flow rate measurement was tested in an air-flow test loop with different test sections to produce asymmetric flow profiles (Figure 4). All pipes have a diameter of $0.08\ \mathrm{m}$. Air comes through an inlet pipe of $6\ L/D$ length, which contains a baffle plate and a flow straightener to form a uniform flow profile. Then the air flow enters an interchangeable bend installation (elbow, double elbow, T-junction) and $0.8\,L/D$ downstream the flow rate sensor. A subsequent straight outlet pipe of $6\,L/D$ prevents any dynamic pressure interference from the outlet. The inflow velocity was controlled via a mass flow controller in a range between 0.5 m/s and 4.0 m/s in steps of 0.5 m/s at reference conditions ($p = 1.013\ \mathrm{bar}$, $\vartheta = 25\ °\mathrm{C}$). The measurements were performed at steady state flow conditions.

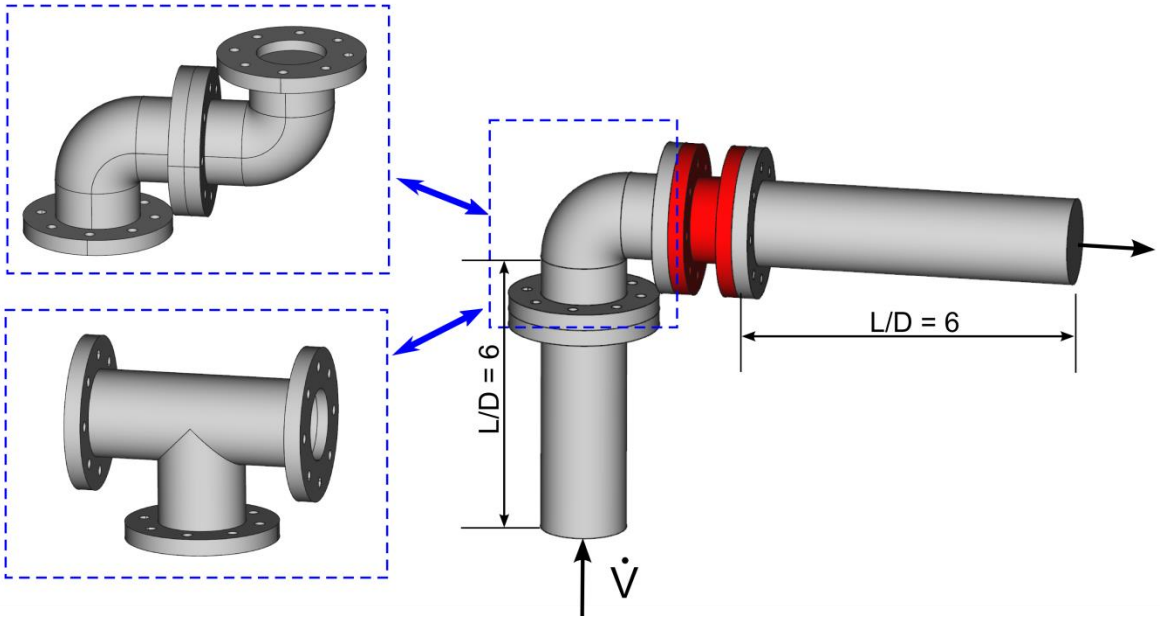

Figure 4. Test setup with interchangeable bends and the sensor (red).

3.2 Results

Figure 5 shows exemplarily the measured spatial velocity distribution for the three pipe configurations at a nominal inlet velocity $v_{\mathrm{nom}} = 3.0\ \mathrm{m/s}$. The sectional views were created by linear interpolation between the local measurement points (indicated by the black dots) and the pipe wall. Additionally, the radial profiles of the velocity on the two radii r_1 and r_2 are given in the plots below. For all configurations a strong flow asymmetry with higher velocities in the upper part of the cross section were found. The maximum and minimum relative deviation from the average $\bar{v}$ is 26.9% and -21.7 % for the T-junction.

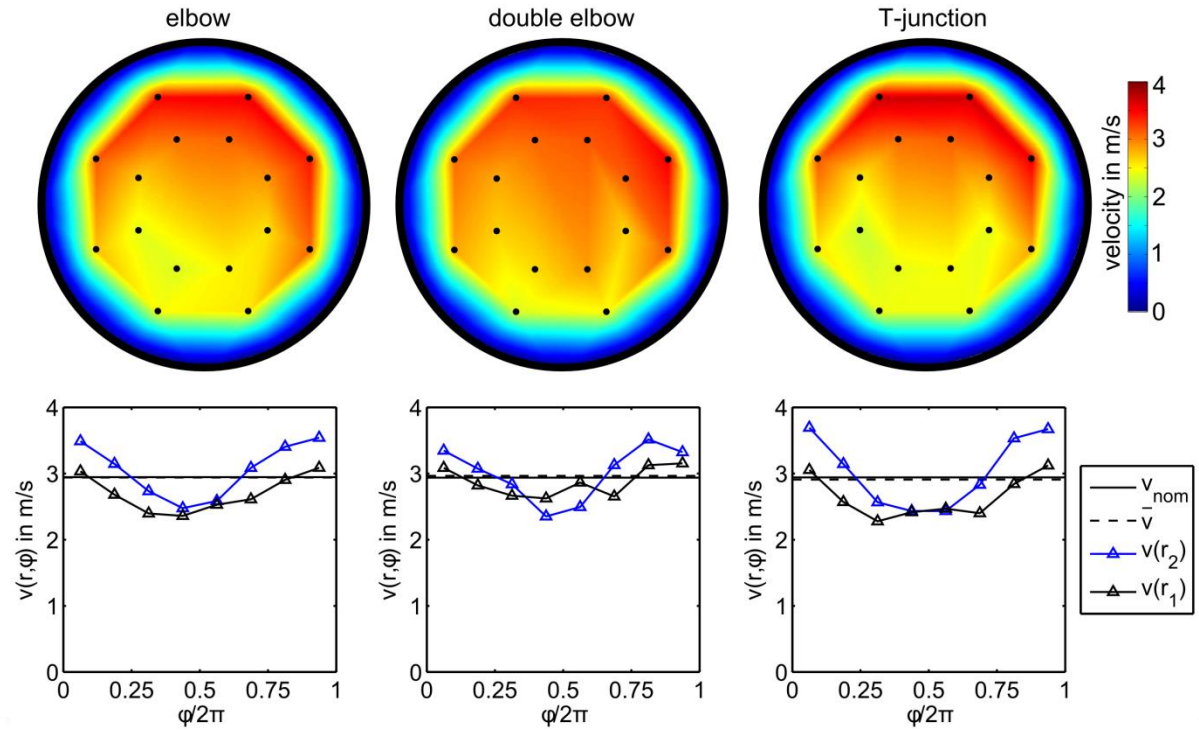

Figure 5. Distribution maps and radial profiles of the measured local flow velocities for the three pipe configurations and $v_{\mathrm{nom}} = 3.0\ \mathrm{m/s}$.

One measure for the grade of the asymmetry in the flow profile is the coefficient of variation $c_v = s/\bar{v}$ with the standard deviation s. From Figure 6 it is evident that c_v increases with increasing velocity v_{nom}. The strongest unbalance can be found for the T-junction configuration.

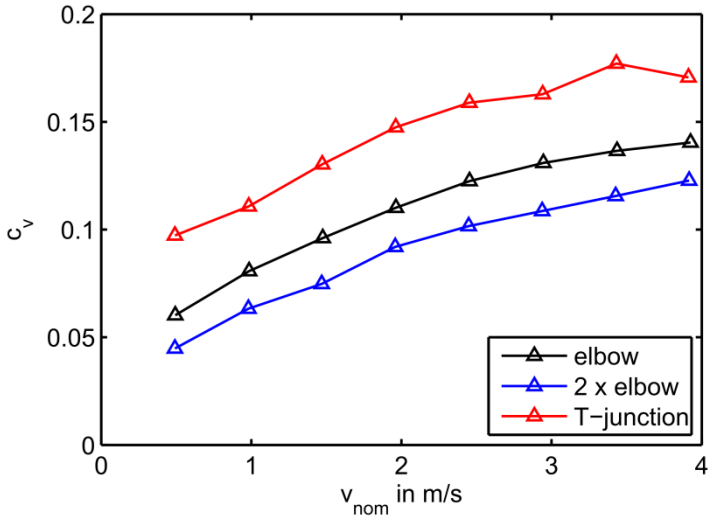

Figure 6. Coefficient of variation c_v as a function of v_{nom} for the three pipe configurations.

The actual correctness of the measured flow rate can be expressed by the relative deviation $f = (\bar{v} - v_{\mathrm{nom}})/v_{\mathrm{nom}}$. Figure 7 shows the uncertainties for the three configurations in the investigated range of nominal velocities. They are mainly within a range of $|f| < 2\ \%$. A significant dependence on flow rate or asymmetry is not observable. The measurement uncertainty was determined via a repeated measurement. $\bar{v}$ was exemplary measured seven times for the T-junction configuration with a nominal value of $v_{\mathrm{nom}} = 2.91\ \mathrm{m/s}$. The coefficient of variation was $c_v = 0.00975$ with an averaged value of $\bar{v} = 2.87\ \mathrm{m/s}$ and a standard deviation of $s = 0.028\ \mathrm{m/s}$ over all seven measurements.

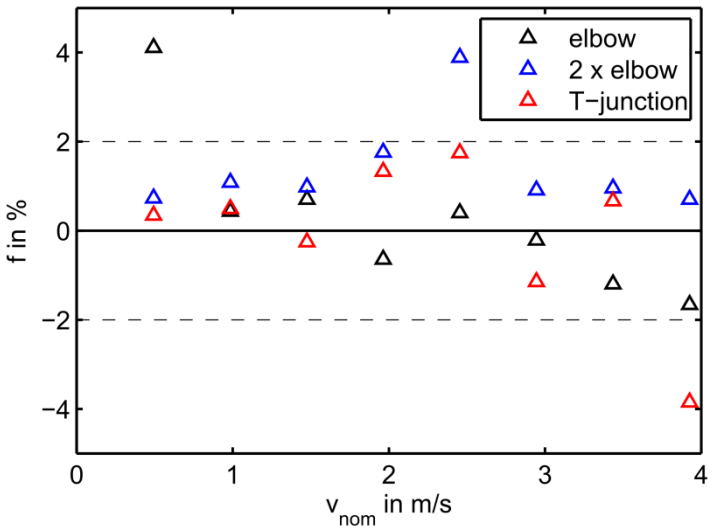

Figure 7. Measured relative deviation from nominal velocity.

Within this proof of principle study the general applicability of the TAGS for flow measurement in asymmetric flow profiles directly downstream of pipe bends was demonstrated. For a further

reduction of the measurement uncertainty a sophisticated analysis of the measurement point distribution, calibration procedure and data processing electronics is necessary.

4 SUMMARY AND CONCLUSIONS

In this present paper we presented a new method and device for the measurement of flow rates for non-symmetric flow profiles, such as directly downstream of pipe bends and other installations in a pipe. The approach bases on a thermal anemometry grid sensor (TAGS) that measures local flow velocities at multiple locations in the flow cross-section simultaneously. Applicability was demonstrated and accuracy as well as uncertainty was determined for three exemplary for three pipe bend configurations and air flow. A deviation of the measured flow rate $< 2\,\%$ at $0.8\ \mathrm{L/D}$ downstream the bends was found.

5 ACKNOWLEDGEMENTS

This work was carried out in part within the research projects “SINABEL (funded by the German Federal Ministry of Education and Research (BMBF) under the contract number 02NUK027E) and “EVanS” (funded by the German Federal Ministry of Economic Affairs and Energy under the contract number 03THW12H02) . Responsibility for the content of this publication lies with the authors.

6 REFERENCES

[1] *ISO 5167:2003 Measurement of fluid flow by means of pressure differential devices inserted in circular cross-section conduits running full*.

[2] C.N.B. Martin, "Effects of upstream bends and valves on oriffice plate pressure distributions and discharge coefficients", *International Journal of Heat and Fluid Flow*, **3**, pp. 135–141 (1982).

[3] S.B.M. Beck and J. Mazille, "A study of a pressure differential flow meter that is insensitive to inlet conditions", *Flow Measurement and Instrumentation*, **12**, pp. 379–384 (2002).

[4] C. Ruppel and F. Peters, "Effects of upstream installations on the reading of an ultrasonic flowmeter", *Flow Measurement and Instrumentation*, **15**, pp. 167–177 (2004).

[5] M. Holm, J. Stang and J. Delsing, "Simulation of flow meter calibration factors for various installation effects", *Measurement*, **15**, pp. 235–244 (1995).

[6] I. Care, F. Bonthoux and J.-R. Fontaine, "Measurement of air flow in duct by velocity measurements", *European Physical Journal Web of Conferences* ,Vol. 77 ,(2014).

[7] D. Wecel, T. Chmielniak and J. Kotowicz, "Experimental and numerical investigations of the averaging Pitot tube and analysis of installation effects on the flow coefficient", *Flow Measurement and Instrumentation*, **19**, pp. 301–306 (2008).

[8] *IEC 60751*,Industrial platinum resistance thermometers and platinum temperature sensors,(2008).

[9] H.H. Bruun, *Hot wire anemometry: principles and signal analysis*,Oxford Univ. Pr.,Oxford, United Kingdom,(1996).

[10] M. Arlit, E. Schleicher and U. Hampel, "Thermal Anemometry Grid Sensor", *Sensors*, **17**, (2017).

[11] *ISO 3966:2008*,Measurement of fluid flow in closed conduits – Velocity area method using Pitot static tubes.

[12] M. Arlit, U. Hampel and C. Schroth, *Durchflussmessanordnung und strömungstechnische Anordnung*, DE102019103674.7, 2019.